Interplay between hydrodynamic and Brownian fluctuations in sedimenting colloidal suspensions

J. T. Padding[1,2] and A. A. Louis[2,3]
[1]Computational Biophysics, University of Twente, P.O. Box 217, 7500 AE, Enschede, The Netherlands
[2]Department of Chemistry, Cambridge University, Lensfield Road, Cambridge CB2 1EW, United Kingdom
[3]Rudolf Peierls Centre for Theoretical Physics, 1 Keble Road, Oxford OX1 3NP, United Kingdom
(Received 19 October 2007; published 22 January 2008)

We apply a hybrid molecular dynamics and mesoscopic simulation technique to study the steady-state sedimentation of hard sphere particles for Peclet number (Pe) ranging from 0.08 to 12. Hydrodynamic backflow causes a reduction of the average sedimentation velocity relative to the Stokes velocity. We find that this effect is independent of Pe number. Velocity fluctuations show the expected effects of thermal fluctuations at short correlation times. At longer times, nonequilibrium hydrodynamic fluctuations are visible, and their character appears to be independent of the thermal fluctuations. The hydrodynamic fluctuations dominate the diffusive behavior even for modest Pe number, while conversely the short-time fluctuations are dominated by thermal effects for surprisingly large Pe numbers. Inspired by recent experiments, we also study finite sedimentation in a horizontal planar slit. In our simulations distinct lateral patterns emerge, in agreement with observations in the experiments.

DOI: 10.1103/PhysRevE.77.011402 PACS number(s): 82.70.Dd, 05.40.−a, 47.11.−j, 47.20.Bp

I. INTRODUCTION

The steady-state sedimentation of spheres in a viscous medium at low Reynolds (Re) number is an important model problem in nonequilibrium statistical mechanics, exhibiting subtle and interesting physics [1–3]. Some properties are relatively straightforward to determine. For example, the sedimentation velocity V_S^0 of a single sphere was calculated over 150 years ago by Stokes [4] to be $V_S^0=\frac{2}{9}ga^2(\rho_c-\rho)/\eta$, where a and ρ_c are the radius and density of the sphere, g is the gravitational acceleration, and ρ and η are the density and viscosity of the fluid. On the other hand, even the first-order effect of finite volume fraction $\phi=\frac{4}{3}\pi n_c a^3$ (n_c is the particle number density) was not calculated until 1972 when Batchelor [5] showed that

$$V_S = V_S^0[1 - 6.55\phi + (O\phi^2)]. \tag{1}$$

The effect of a finite volume fraction on sedimentation is dominated by long-ranged hydrodynamic forces that decay with interparticle distance r as slowly as r^{-1}. These forces are hard to treat analytically because they can easily lead to spurious divergences. Equation (1) also highlights the strong effect of the hydrodynamic forces. For example, a naive application of this lowest order result would suggest that all sedimentation should stop at $\phi\approx 0.15$. Of course this is not true since there are important higher-order corrections in ϕ whose calculation remains an active topic of research [6].

If the influence of hydrodynamics on the average sedimentation velocity at finite volume fraction is nontrivial to calculate, then the fluctuations around that average would appear even more formidable to determine. In a remarkable paper, Caflisch and Luke [7] used a simple scaling argument to predict that, for a homogeneous suspension, the velocity fluctuations $\delta V=V-V_S$ should diverge as $\langle \delta V^2\rangle \sim L$, where L is the smallest container size. This surprising result stimulated much theoretical and experimental work, as well as no small amount of controversy [2]. Particle velocimetry experiments clearly show the existence of large-scale velocity fluctuations, which manifest as "swirls" [8–12]. The experiments of Nicolai *et al.* [8] and Segrè *et al.* [9] suggest that while for small containers the velocity fluctuations do indeed grow linearly in L, for larger containers the velocity fluctuations saturate (see, however, [11,13]). The reasons (if any) that this should be observed have been the subject of sustained theoretical debate. It was shown by Koch and Shaqfeh [14] that hydrodynamic interactions can be screened if the colloids exhibit certain long-ranged correlations reminiscent of those found for electrostatic systems. A number of theories have been proposed to generate such correlations in the bulk, including a coupled convective-diffusion model by Levine *et al.* [15] that generates a noise-induced phase transition to a screened phase. Another class of theories focuses on the container walls. For example Hinch [16] has argued that the bottom of a vessel will act as a sink for fluctuations, a prediction that appears to be confirmed by computer simulations [17,18]. Other authors have emphasized the importance of stratification [12,19–22] and polydispersity [18,23].

Most of the theoretical studies of sedimentation described above have focused on the non-Brownian limit where thermal fluctuations are negligible. This can be quantified by defining the Peclet number (Pe)

$$\mathrm{Pe} = \frac{V_S^0 a}{D_0} = \frac{M_b g a}{k_B T}, \tag{2}$$

where D_0 is the equilibrium self-diffusion constant and $M_b=\frac{4}{3}\pi a^3(\rho_c-\rho)$ is the particle's buoyant mass. The non-Brownian limit then corresponds to $\mathrm{Pe}=\infty$. Because Pe scales as $(\rho_c-\rho)a^4$, the very large Pe numbers needed to approximate the non-Brownian limit are easily achieved by increasing particle size.

The Pe number is directly related to the gravitational length $l_g=k_BT/(M_bg)=a/\mathrm{Pe}$. For this reason, the criterion $\mathrm{Pe}\leqslant 1$ is often used to define the colloidal regime since, roughly speaking, one would expect from the barometric law that particles would then be dispersed throughout the solu-

tion. For example, for polystyrene spheres in water Pe $=O(1)$ for $a \approx 1$ μm. In experiments, the density difference $\Delta\rho=\rho_c-\rho$ can be adjusted by density matching so that the Pe number can also be tuned quite accurately for a given a.

In contrast to most previous theoretical and computational studies, which have focused on the non-Brownian Pe$=\infty$ limit, in this paper we study steady-state sedimentation at the moderate Pe numbers relevant for the colloidal regime. In this regime the particles experience both random thermal fluctuations (caused by random collisions with solvent molecules) and deterministic hydrodynamic fluctuations (fluctuations in the sedimentation velocity of individual colloids caused by multibody hydrodynamic interactions). A key question will be how these two kinds of fluctuations interact.

We employ stochastic rotation dynamics (SRD) [24–26] to describe the solvent, and a molecular dynamics (MD) scheme to propagate the colloids. Such a hybrid technique was employed by Malevanets and Kapral [27], and recently used to study colloidal sedimentation by ourselves [28] and by Hecht *et al.* [29]. In Sec. II we briefly recap the salient details of our simulation method.

In Sec. III we study the average sedimentation velocity. Our principle finding is that this follows exactly the same trend with volume fraction ϕ as found for the Pe$=\infty$ non-Brownian limit. In other words, the effects of backflow are completely dominated by the hydrodynamic interactions (HI), even when the Brownian forces are, on average, much stronger. In Secs. IV and V we investigate in some detail the velocity fluctuations $\langle \delta V^2 \rangle$. We find that the thermal and hydrodynamic fluctuations appear to act independently of each other. Their effects are additive, at least in the accessed simulation regime, where the hydrodynamic fluctuations are unscreened. Some of these results have appeared earlier [28], but here they are treated in much more detail. In Sec. VI we calculate the self-diffusion coefficient, highlighting the effects of hydrodynamic dispersion. In Sec. VII we briefly consider the case of finite sedimentation in a horizontal planar slit. We observe distinct lateral patterns, in agreement with recent laser scanning confocal microscopy. In Sec. VIII we discuss the importance of thermal fluctuations over hydrodynamic fluctuations. Finally, in Sec. IX we present our conclusions.

II. HYBRID MD-SRD COARSE-GRAINED SIMULATION METHOD

The time- and length-scale differences between colloidal and solvent particles are enormous: a typical colloid of diameter 1 μm will displace on the order of 10^{10} water molecules. Clearly, some form of *coarse graining* of the solvent is necessary. In this paper we use SRD to efficiently describe the dynamics of the solvent. The colloids are coupled to the solvent through explicit interaction potentials. We have recently performed an extensive validation of this method [26]. We will therefore only reproduce the most important conclusions.

A. Solvent-solvent interactions

In SRD, the solvent is represented by a large number N_f of pointlike particles of mass m_f. We will call these *fluid* particles, with the caveat that, however tempting, they should not be viewed as some kind of composite particles or clusters made up of the underlying molecular fluid. The particles are merely a convenient computational device to facilitate the coarse graining of the fluid properties [26].

In the first step, the positions and velocities of the fluid particles are propagated by integrating Newton's equations of motion. The forces on the fluid particles are generated by external forces generated by gravity, walls, or colloids. Direct forces between pairs of fluid particles are, however, excluded; this is the main reason for the efficiency of the method. After propagating the fluid particles for a time Δt_c, the second step of the algorithm simulates the collisions between fluid particles. The system is partitioned into cubic cells of volume a_0^3. The velocities relative to the center of mass velocity $\mathbf{v}_{\mathrm{cm}}$ of each separate cell are then rotated,

$$\mathbf{v}_i \mapsto \mathbf{v}_{\mathrm{cm}} + \mathbf{R}(\mathbf{v}_i - \mathbf{v}_{\mathrm{cm}}). \tag{3}$$

$\mathbf{R}$ is a rotation matrix which rotates velocities by a fixed angle α around a randomly oriented axis. The angle α can be anything between 0 and 180 degrees, but too small angles should be avoided because in the limit of zero angle there are no collisions and thermal equilibrium cannot be achieved. The aim of the collision step is to transfer momentum between the fluid particles. The rotation procedure can thus be viewed as a coarse graining of particle collisions over time and space. Because mass, momentum, and energy are conserved locally, the correct (Navier-Stokes) hydrodynamic equations are captured in the continuum limit, *including* the effect of thermal noise [24].

Ihle and Kroll [25] pointed out that at low temperatures or small collision times Δt_c the transport coefficients of SRD show anomalies. These anomalies are caused by the fact that fluid particles in a given cell can remain in that cell and participate in several collision steps. They showed that under these circumstances the assumption of molecular chaos and Galilean invariance are incorrect. They also showed how the anomaly can be entirely cured by applying a random shift of the cell coordinates before the collision step. It is then possible to analytically calculate the shear viscosity of the SRD fluid [30]. Such expressions are very useful because they enable us to efficiently tune the viscosity of the fluid, without the need of trial and error simulations.

B. Colloid-colloid and colloid-solvent interactions

In the simulation, colloidal spheres of mass M are propagated through the velocity Verlet algorithm [31] with a time step Δt_{MD}. The colloids are embedded in the fluid, and interact with the fluid particles through a repulsive (Weeks-Chandler-Andersen) potential,

$$\varphi_{cf}(r) = \begin{cases} 4\epsilon\left[\left(\dfrac{\sigma_{cf}}{r}\right)^{12} - \left(\dfrac{\sigma_{cf}}{r}\right)^{6} + \dfrac{1}{4}\right] & (r \leqslant 2^{1/6}\sigma_{cf}), \\ 0 & (r > 2^{1/6}\sigma_{cf}). \end{cases} \tag{4}$$

The colloid-colloid interaction is represented by a similar, but steeper, repulsive potential,

$$\varphi_{cc}(r) = \begin{cases} 4\epsilon\left[\left(\frac{\sigma_{cc}}{r}\right)^{48} - \left(\frac{\sigma_{cc}}{r}\right)^{24} + \frac{1}{4}\right] & (r \leqslant 2^{1/24}\sigma_{cc}), \\ 0 & (r > 2^{1/24}\sigma_{cc}). \end{cases} \tag{5}$$

As long as the colloid-colloid interactions are hard enough, the precise way in which the interactions are achieved does not matter. Here we have chosen the exponents (48 and 24) as high as possible, yet low enough to enable accurate integration of the equations of motion with a time step Δt_{MD} close to the collision time interval Δt_c. Details can be found in Ref. [26].

Because the surface of a colloid is never perfectly smooth, collisions with fluid particles transfer angular as well as linear momentum. These interactions may be approximated by stick boundary conditions. We have studied several implementations of stick boundary conditions for spherical colloids [32] and derived a version of stochastic boundary conditions which reproduce linear and angular momentum correlation functions that agree with Enskog theory for short times and hydrodynamic mode-coupling theory for long times. Nevertheless, to comply with Ref. [24], in this paper we use the radial interactions described in Eq. (4). These do not transfer angular momentum to a spherical colloid and so induce effective slip boundary conditions. For many of the hydrodynamic effects we will discuss here the difference with stick boundary conditions is quantitative, not qualitative, and also well understood. For example, we have confirmed that the flowfield around a single sedimenting sphere decays, to first order, such as $a/(2r)$ for a slip boundary sphere [26], whereas it decays similar to $3a/(4r)$ for a stick boundary sphere.

To avoid (uncontrolled) depletion forces, we routinely choose the colloid-fluid interaction range σ_{cf} slightly below half the colloid diameter $\sigma_{cc}/2$ [26]. There is no *a priori* reason why the hydrodynamic radius should be exactly half the particle-particle hard-core diameter for a physical system. For charged systems, for example, the difference may be substantial. An additional advantage of this choice is that more fluid particles will fit in the space between two colloids, and consequently lubrication forces will be more accurately represented between the hydrodynamic cores. We have confirmed that with our parameters SRD resolves the analytically known lubrication forces down to gap widths as small as $a/5$. The agreement at small distances is caused also by repetitive collisions of the fluid particles trapped between the two surfaces. But at some point the lubrication force will break down: for example, when only one or two SRD particles are left in the gap between two surfaces, the SRD fluid no longer represents a continuous viscous medium. An explicit correction could be applied to correctly resolve these forces for very small distances, as was implemented by Nguyen and Ladd [33] for lattice Boltzmann dynamics. However, in this paper our choice of σ_{cf} is small enough for SRD to sufficiently resolve lubrication forces up to the point where the direct colloid-colloid interactions start to dominate [26].

C. Time scales and hydrodynamic numbers

Many different time scales govern the physics of a colloid of mass M embedded in a solvent. Hydrodynamic interactions propagate by momentum diffusion and also by sound. The sonic time is the time it takes a sound wave to travel the radius of a colloid, $t_{cs}=a/c_s$, where c_s is the speed of sound. The kinematic time, on the other hand, is the time it takes momentum to diffuse over the radius of a colloid, $\tau_\nu=a^2/\nu$, where ν is the kinematic viscosity of the solvent. For a colloid of radius $a=1$ μm in water, $\tau_{cs}\approx 10^{-9}$ s and $\tau_\nu \approx 10^{-6}$ s.

The next time scale is the Brownian time $\tau_B=M/\xi_S$, where $\xi_S=6\pi\eta a$ is the Stokes friction for stick boundary conditions, or $4\pi\eta a$ for slip boundary conditions. It measures the time for a colloid to lose memory of its velocity (see, however, [26]). The most relevant time scale for Brownian motion is the diffusion time $\tau_D=a^2/D_0$, which measures how long it takes for a colloid to diffuse over a distance a in the absence of flow. For a colloid of $a=1$ μm in water, $\tau_D \approx 5$ s.

When studying sedimentation, the Stokes time is the time it takes a single colloid to advect over its own radius, $t_S=a/V_S^0$. The Stokes time and the diffusion time are related by the Peclet number: $\mathrm{Pe}=\tau_D/t_S$. If $\mathrm{Pe}\gg 1$, then the colloid moves convectively over a distance much larger than its radius a in the time τ_D that it diffused over the same distance. For $\mathrm{Pe}\ll 1$, on the other hand, the opposite is the case, and the main transport mechanism is diffusive. It is sometimes thought that for low Pe numbers hydrodynamic effects can safely be ignored, but this is not always true, as we will show.

In summary, in colloidal suspensions we encounter a range of time scales, ordered similar to $t_{cs}<\tau_B<\tau_\nu<(\tau_D,t_S)$, where t_S may be smaller or larger than τ_D depending on Pe, and where we have assumed $\rho_c\approx\rho$ to justify $\tau_B<\tau_\nu$. The entire range of time scales can span more than 10 orders of magnitude. Thankfully, it is not necessary to exactly reproduce each of the different time scales in order to achieve a correct coarse graining of colloidal dynamics. We can "telescope down"[26] the relevant time scales to a hierarchy which is compacted to maximize simulation efficiency, but sufficiently separated to correctly resolve the underlying physical behavior. Keeping the relevant time scales an separated by about an order of magnitude should suffice.

Similar arguments can be made for various hydrodynamic numbers. For example, the Re number of sedimenting colloidal particles is normally very low, on the order of 10^{-5} or less. But there is no need to take such a low value since many relative deviations from the zero-Re Stokes regime scale with Re^2. Exactly how big an error one makes depends on what one is investigating, but for our purposes we will take $\mathrm{Re}\leqslant 0.4$ as an upper bound. We have shown [26] that for the friction on a sphere inertial effects are unimportant up to $\mathrm{Re}\approx 1$. We note that our upper bound on Re also ensures that the time hierarchy condition $\tau_\nu<(t_S,\tau_D)$ is fulfilled. In principle Pe can be whatever we like as long as Re remains low and the hierarchy is obeyed.

To achieve the hierarchy of time scales and hydrodynamic numbers, in our simulations we choose an average number of

fluid particles per collision volume equal to $\gamma=5$, a collision interval $\Delta t_c=0.1$ (in units of $t_0=a_0\sqrt{m_f/k_BT}$), and a rotation angle $\alpha=\pi/2$, leading to a kinematic viscosity $\nu=0.5\ a_0^2/t_0$. We choose a colloidal mass $M=125m_f$, and interaction parameters $\sigma_{cf}=2a_0$, $\sigma_{cc}=4.3a_0$, and $\epsilon=2.5k_BT$. For an extensive discussion of the choice of parameters, see Ref. [26]. We have verified that this choice leads to a small relative error in the full velocity field, and that we can quantitatively calculate the observed friction on a colloid [26]. Note that this friction is somewhat lower than expected on the basis of a hydrodynamic radius set equal to $\sigma_{cf}=2a_0$. This is due to additional Enskog friction effects, where the different contributions to the friction add "in parallel," as explained in Ref. [26]. The resulting effective hydrodynamic radius $a=1.55a_0$ will be used throughout this paper. We note that, because $a<\sigma_{cc}/2$, we cannot study hydrodynamic volume fractions ϕ far beyond 0.25. Beyond this limit, steric interactions between the colloids start to dominate. We therefore limit ourselves to low volume fractions ($\phi<0.13$). The time scales in our simulations are well separated: $t_{cs}=1.2t_0$, $\tau_B=2.5t_0$, $\tau_\nu=4.8t_0$, and $\tau_D=120t_0$.

III. AVERAGE SEDIMENTATION VELOCITY

Sedimentation simulations were performed in a periodic box of dimensions $L_x=L_y=32a_0$ and $L_z=96a_0$ (approximately $21\times21\times62a$), with periodic boundaries in all directions, containing $N=8$ to 800 colloids. The number of SRD particles was adjusted so that the free volume outside the colloids contained an average of 5 particles per coarse-graining cell volume a_0^3. This corresponds to a maximum of $N_f\approx5\times10^5$ SRD particles. A gravitational field g, applied to the colloids in the z direction, was varied to produce different Peclet numbers, ranging from Pe=0.08 to Pe=12. At the same time the Reynolds numbers ranged from Re=0.003 to 0.4. The absence of walls necessitates an additional constraint to keep the system from accelerating indefinitely. One could for example constrain the center-of-mass of the solvent or the center-of-mass of the entire system. However, in most experiments a wall is present at the bottom of the vessel (sufficiently tall vessels are needed to study steady-state sedimentation). The wall at the bottom and the incompressibility of the fluid together enforce a total volume flux of zero at every height in the vessel. Because of the density difference between colloids and fluid this leads to a motion of the center-of-mass. To stay close to the experimental situation, the average sedimentation velocity V_S reported here is obtained in a frame of reference in which the downward volume flux $\phi_c V_S$ of colloids is exactly balanced by the upward flux $(1-\phi_c)V_f$ of fluid. Here $\phi_c=(\frac{4}{3}\pi N\sigma_{cc}^3)/(L_xL_yL_z)$ is the volume fraction excluded to the solvent by the presence of the colloids, and V_f is the average velocity of the fluid.

Right after the simulations start, the colloidal positions and velocities have not yet acquired their steady-state distributions. We monitored block averages (in time) of the sedimentation velocity and the behavior of sedimentation velocity fluctuations, which will be discussed in the next section. We verified that there was no drift in these properties after about 100 Stokes times t_S, corresponding to sedimentation down the height of about two periodic boxes. The absence of any drift indicated that the suspensions were now in steady state.

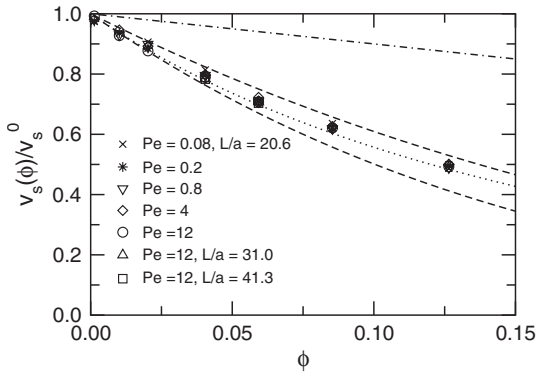

FIG. 1. Average sedimentation velocity, V_S normalized by the Stokes velocity V_S^0, as a function of volume fraction ϕ for various Peclet numbers and system sizes. Dashed lines correspond to the semiempirical Richardson-Zaki law $(1-\phi)^n$, with $n=4.7$ for the upper and $n=6.55$ for the lower line. The dotted line is another theoretical prediction taking higher order HI into account [6]. Ignoring hydrodynamics leads to $V_S/V_S^0=1-\phi$ (dashed-dotted line).

The simulations were subsequently run between 200 t_S for Pe=0.08 to 30 000 t_S for Pe=12. To check that our system is large enough, we performed some runs for 1.5 and 2 times the box size described above, finding no significant changes in our conclusions.

The average sedimentation velocity V_S for different Peclet numbers and system sizes as a function of hydrodynamic packing fraction $\phi=\frac{4}{3}\pi n_c a^3$ is shown in Fig. 1. The results are normalized by the Stokes velocity V_S^0 (the sedimentation velocity of a single particle in the simulation box), resulting in the so-called hindered settling function. At low densities the results are consistent with the result found by Batchelor [5], while at higher densities they compare well with a number of other forms derived for the $\mathrm{Pe}\to\infty$ limit. In most experiments the hindered settling function is well described by the semiempirical Richardson-Zaki law $V_S/V_S^0=(1-\phi)^n$, with n ranging between 4.7 and 6.55 [1,3]. Our results fall between these two extremes. The results compare particularly well with a theoretical prediction by Hayakawa and Ichiki [6], taking higher-order hydrodynamic interactions into account.

One might naively expect that the effect of HI becomes weaker for $\mathrm{Pe}<1$. Taking into account only Brownian forces would result in $V_S=V_S^0(1-\phi)$ (because of flux conservation), which heavily underestimates backflow effects. However, we observe that the results for *all* Peclet numbers $0.08\leqslant\mathrm{Pe}\leqslant12$ lie on the same curve. We emphasis that these results are normalized by the Stokes velocity V_S^0 of a single sphere, which itself decreases with decreasing Peclet number. The important point is that the *additional* hindrance caused by hydrodynamic interactions is observed to be unaffected by the actual Pe number. A reason for this could be that the *average* sedimentation velocity is determined predominantly by the (time-averaged) distribution of distances between the colloids. If this is so, then the particle motion generated by the external field must not lead to a significant change in the

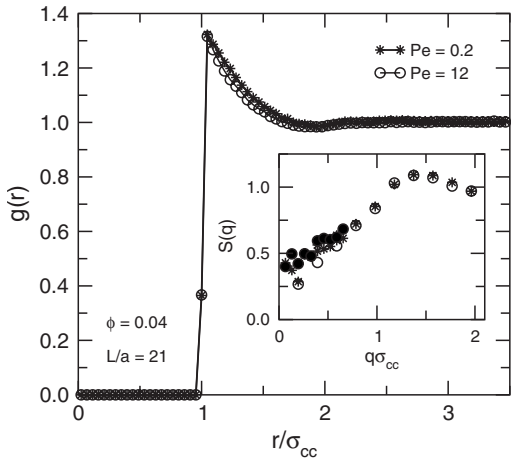

FIG. 2. Main plot: Colloid radial distribution function $g(r)$ for ϕ=0.04 at low (0.2) and high (12) Peclet number. There is no significant difference between the two $g(r)$'s. Inset: Structure factor for the same systems. At Pe=12, small deviations are found for perpendicular (open circles) and parallel (closed circles) wave vectors.

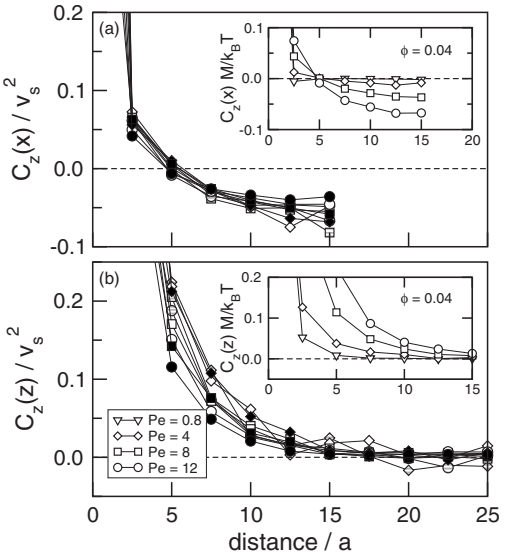

FIG. 3. Spatial correlation functions of the parallel (z) component of the velocity fluctuations as a function of distance perpendicular (a) and parallel (b) to the external field, for three different volume fractions [ϕ=0.02 (grey symbols), ϕ=0.04 (white), ϕ=0.086 (black)] and different Peclet numbers. The correlation functions are scaled with V_S^2 to emphasize hydrodynamic fluctuations. The insets show how $C_z(\mathbf{r})$, scaled with k_BT/M, increases with Pe.

microstructure. That this is indeed the case is shown in Fig. 2, where the main plot shows the colloidal radial distribution function at volume fraction ϕ=0.04 for Peclet numbers 0.2 (stars) and 12 (circles). For Pe=0.2 the result is indistinguishable from equilibrium results, and for Pe=12, despite the fact that the external field is quite strong, the *average* number of neighboring particles at a certain distance from a specific particle changes only very slightly as compared to equilibrium. The inset of Fig. 2 shows the structure factor for the same system. At Pe=12, small deviations are found for perpendicular (open circles) and parallel (closed circles) wave vectors, but again the differences are not very large. Here we already note that all of these systems are in the unscreened regime.

IV. SPATIAL CORRELATIONS IN FLUCTUATIONS

We next discuss velocity fluctuations around the average. In colloidal systems the instantaneous velocity fluctuations $\delta\mathbf{V}=\mathbf{V}-\mathbf{V}_s$ are dominated by thermal fluctuations, with a magnitude determined by equipartition,

$$\Delta V_T^2 = k_BT/M. \tag{6}$$

To disentangle the hydrodynamic fluctuations from thermal fluctuations, we describe spatial and temporal correlations in the velocity fluctuations. The spatial correlation of the z component (parallel to the sedimentation direction) of the velocity fluctuations can be defined as

$$C_z(\mathbf{r}) \equiv \langle \delta V_z(\mathbf{0})\, \delta V_z(\mathbf{r}) \rangle, \tag{7}$$

where $\langle \cdots \rangle$ represents an average over time and over all colloids. The distance vector $\mathbf{r}$ is taken perpendicular to sedimentation, $C_z(x)$, or parallel to it, $C_z(z)$. Note that we will not normalize the correlation functions by their initial values. Rather, we will normalize them by values which have a more physical meaning, such as the squared sedimentation velocity V_S^2, or the thermal fluctuation strength k_BT/M.

In Fig. 3 we plot $C_z(\mathbf{r})$, which shows a positive spatial correlation along the direction of flow, and an anticorrelation perpendicular to the flow, very much similar to that observed in the experiments of Nicolai *et al.* [8]. The inset of Fig. 3(a) shows that at Pe=0.8 the correlation in the perpendicular direction, $C_z(x)$, is almost negligible compared with the thermal fluctuation strength k_BT/M, whereas for larger Pe, distinct regions of negative amplitude emerge, which grow with increasing Pe. Similarly, the inset of Fig. 3(b) shows correlations in the parallel direction that rapidly increase with Pe. For the highest Peclet numbers studied ($4 \leqslant \mathrm{Pe} \leqslant 12$), the amplitudes of these correlations grow proportionally to V_S^2, as shown in the main plots of Fig. 3. Unfortunately, because the division by V_S^2 amplifies the statistical noise, we are unable to verify whether this scaling persists for Pe$<$4. The minimum in Fig. 3(a) is at about half the box width (this is also the reason why no data points could be collected for $x \geqslant 15a$). This suggests that the velocity fluctuations are unscreened and only limited by our box dimensions (see [34]). We confirm this in Fig. 4, where it is seen that the correlation length scales linearly with box dimensions.

V. TEMPORAL CORRELATIONS IN FLUCTUATIONS

Similarly to the spatial correlations of the previous section, the temporal correlation of the z component of the velocity fluctuations can be defined as

$$C_z(t) \equiv \langle \delta V_z(0)\, \delta V_z(t) \rangle, \tag{8}$$

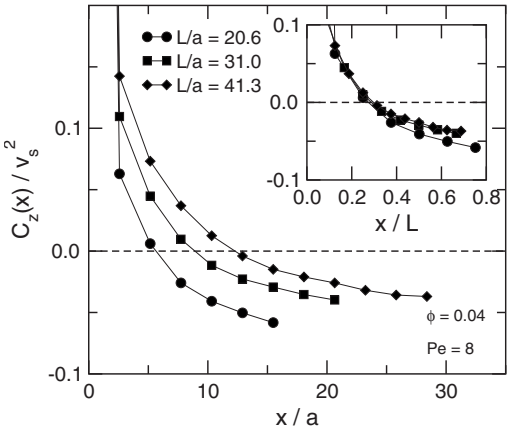

FIG. 4. Spatial correlation functions of the parallel (z) component of the velocity fluctuations as a function of distance perpendicular to the external field, for different system sizes. In the inset, distance is scaled with the horizontal box size L. All simulations were performed at ϕ=0.04 and Pe=8.

where now t is a correlation time and $\langle \cdots \rangle$ denotes an average over all colloids and all time *origins*. Figure 5 shows the temporal correlation functions along the direction of sedimentation on a linear scale. Clearly the correlation is increasing with increasing Pe number. To investigate this in more detail, we plot the temporal correlation on a log-log and log-linear plot in Fig. 6.

At very short times the velocity decorrelation is quantitatively described by Enskog dense-gas kinetic theory [35,36], which predicts the following decay:

$$\lim_{t\to 0} C_z(t) = \Delta V_T^2 \exp(-t\xi_E/M), \tag{9}$$

where the Enskog friction coefficient is given by

$$\xi_E = \frac{8}{3}\left(\frac{2\pi k_B T M m_f}{M+m_f}\right)^{1/2} \gamma \sigma_{cf}^2. \tag{10}$$

Equation (9) describes the velocity relaxation due to random collisions with the solvent particles.

At intermediate times the temporal correlation follows the well-known algebraic long-time tail

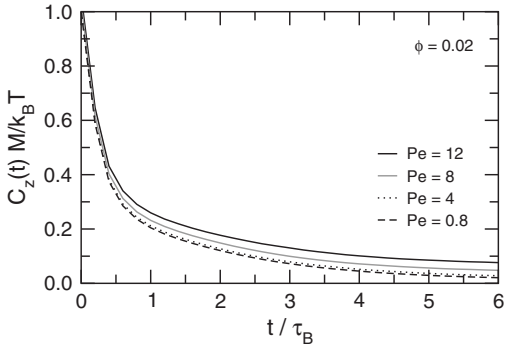

FIG. 5. Temporal correlation functions of the z component of the velocity fluctuations for ϕ=0.02 and different Peclet numbers. Time is scaled with the Brownian relaxation time $\tau_B = M/\xi$ and the velocities are scaled with the thermal fluctuation strength k_BT/M.

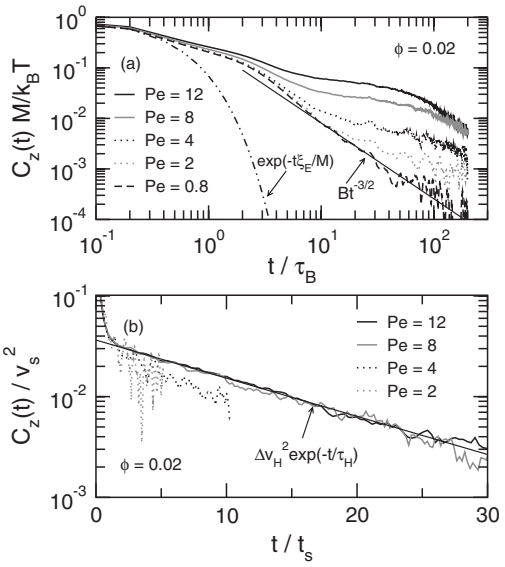

FIG. 6. Temporal correlation functions of the z component of the velocity fluctuations for ϕ=0.02 and different Peclet numbers. (a) Time is scaled with the Brownian relaxation time $\tau_B = M/\xi$ and the velocities are scaled with the thermal fluctuation strength k_BT/M. The straight line is the hydrodynamic long time tail $Bt^{-3/2}$ with $B^{-1} = 12\rho k_BT(\pi\nu)^{3/2}$ [37]. The results for Pe$\leqslant$1 are indistinguishable. (b) Time is scaled with the Stokes time $t_S = a/V_S$ and the velocities are scaled with V_S^2 to highlight hydrodynamic velocity fluctuations. The straight line is a fit demonstrating the exponential decay of nonequilibrium hydrodynamic fluctuations.

$$C_{long}(t) = Bt^{-3/2}, \tag{11}$$

associated with the fact that momentum fluctuations diffuse away at a finite rate determined by the kinematic viscosity ν. Analytical mode-coupling calculations yield a prefactor $B^{-1} = 12\rho k_BT(\pi/\nu)^{3/2}$ [37]. This exactly fits the low Pe ($\leqslant$1) results in Fig. 6(a) with no adjustable parameters. We note that similar agreement was found for the long-time tails for other parameter choices [32] at equilibrium. Of course, these simulations are all at finite Pe number, and so are out of equilibrium, but for small Pe the long-time tail dominates within the simulation accuracy that we obtain.

In an experimental study on the sedimentation of non-Brownian (Pe$\to\infty$) particles, Nicolai *et al.* [8] found an exponential temporal relaxation of the form

$$C_z(t) = \Delta V_H^2 \exp(-t/\tau_H). \tag{12}$$

This nonequilibrium hydrodynamic effect takes place over much longer time scales than the initial exponential relaxation due to random collisions with the solvent particles, i.e., $\tau_H \gg M/\xi_E$. The double-logarithmic figure 6(a) shows that a new mode of fluctuations becomes distinguishable in our simulations for Pe$>$1. In the log-linear figure 6(b) the correlation functions are scaled with V_S^2 to highlight the nonequilibrium hydrodynamic fluctuations. For Pe$\geqslant$8 the fluctuations scale onto a single exponential master curve, similar to the high-Pe experiments of Nicolai *et al.* [8], whereas for lower Pe deviations are seen. From the exponential fit to Eq. (12), we can estimate the relaxation time τ_H and the ampli-

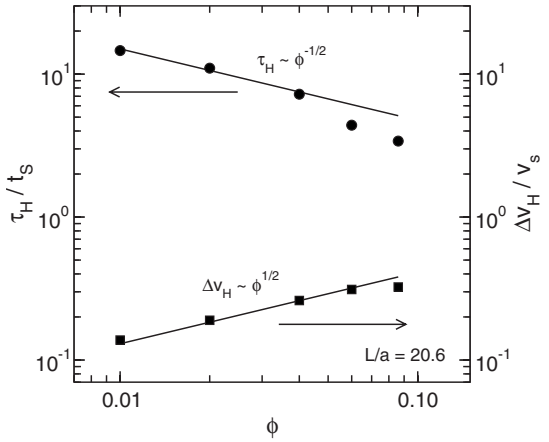

FIG. 7. Scaling of the hydrodynamic relaxation times (left scale) and velocity fluctuation amplitudes (right scale) with volume fraction. Straight lines are expected scalings for an unscreened system [7,38].

tude ΔV_H^2 of the hydrodynamic fluctuations. These are shown in Fig. 7 for different volume fractions ϕ, and in Fig. 8 for different box sizes L/a. The results are consistent with a scaling $\Delta V_H/V_S \propto \sqrt{L\phi/a}$ and $\tau_H/t_S \propto \sqrt{L/(\phi a)}$.

These scalings can be understood by a simple heuristic argument by Cunha *et al.* [38] akin to that used by Caflisch and Luke [7]: Suppose we consider the box volume to consist of two equally large parts, each with a typical linear dimension of L. The average number of colloids in a volume of size L^3 is $\langle N\rangle = L^3\phi/(\frac{4}{3}\pi a^3)$. Of course the colloids are free to move from one part to the other; the division is entirely artificial. At low enough volume fraction ϕ we assume that the colloidal positions are described by random Poisson statistics. The typical fluctuation in the number of particles will then be of order $\sqrt{\langle N\rangle}$. The extra colloidal weight of order $\sqrt{\langle N\rangle}M_b g$ in one part of the box causes this part to sediment faster than average. This is the hydrodynamic fluctuation referred to before. The extra colloidal weight is balanced by

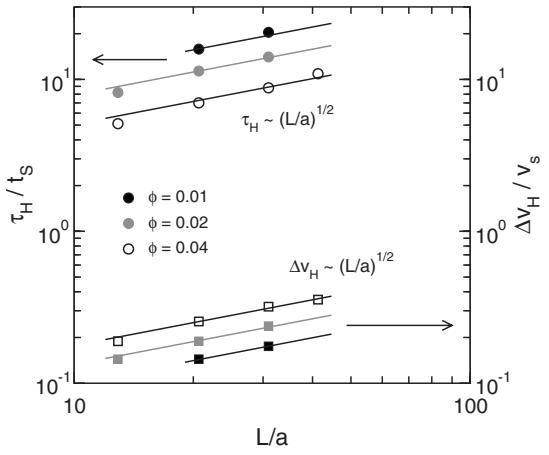

FIG. 8. Scaling of the hydrodynamic relaxation times (left scale) and velocity fluctuation amplitudes (right scale) with box size L. Straight lines are expected scalings for an unscreened system [7,38].

the extra Stokes drag caused by the larger sedimentation velocity, which is of the order of $6\pi\eta L\Delta V_H$. Making use of $V_S = M_b g/(6\pi\eta a)$, we predict for the amplitude of the hydrodynamic fluctuations

$$\Delta V_H^2 = V_S^2 \frac{L\phi}{\frac{4}{3}\pi a}. \tag{13}$$

This is consistent with our observation. Of course the hydrodynamic fluctuation does not persist indefinitely. It will decorrelate on the order of the time needed to fall over its own length, for it will then encounter and mix with a region of average number density. The relaxation time of the hydrodynamic fluctuation is therefore predicted to be

$$\tau_H^2 \approx \frac{L^2}{\Delta V_H^2} = \frac{\frac{4}{3}\pi a L^2}{V_S^2 L\phi} = t_S^2 \frac{\frac{4}{3}\pi L}{a\phi}, \tag{14}$$

where we have used $t_S = a/V_S$.

The above scaling argument does not fix the prefactors. Fitting with the data in Figs. 7 and 8 we find $\Delta V_H \approx 0.29 V_S[\phi(L/a)]^{1/2}$ and $\tau_H \approx 0.33 t_S[\phi(a/L)]^{-1/2}$. It should be noted that the above results concern the velocity fluctuations parallel to the gravitational field (z). In a similar way we have estimated the perpendicular velocity fluctuations to be characterized by $\Delta V_{H,\mathrm{perp}} \approx 0.16 V_S[\phi(L/a)]^{1/2}$ and $\tau_{H,\mathrm{perp}} \approx 0.15 t_S[\phi(a/L)]^{-1/2}$. Note that the ratio of parallel to perpendicular velocity fluctuations is approximately 1.8. This is in agreement with the experimental low ϕ results on non-Brownian spheres by Nicolai *et al.* [8] and by Segrè *et al.* [9], both of whom observed vertical fluctuations approximately twice the horizontal fluctuations in the same range of volume fractions.

VI. DIFFUSION AND DISPERSION

The equilibrium self-diffusion of a colloidal particle is related to its velocity correlation function through the following Green-Kubo equation:

$$D_0(t) = \int_0^t \langle V_x(\tau) V_x(0)\rangle d\tau, \tag{15}$$

where V_x is a Cartesian component of the colloidal velocity. For large enough times t the integral $D_0(t)$ converges to the equilibrium self-diffusion coefficient D_0.

During sedimentation, the diffusion is enhanced by the hydrodynamic fluctuations. In fact, the diffusion is no longer isotropic but tensorial. Focusing first on the component parallel to gravity, we define the parallel diffusion coefficient similarly to Eq. (15) as the large time limit of

$$D_z(t) = \int_0^t \langle \delta V_z(\tau)\delta V_z(0)\rangle d\tau. \tag{16}$$

In Fig. 9 we show $D_z(t)$ normalized by the equilibrium value D_0 for a range of Pe numbers. Note that even though the hydrodynamic fluctuations may be small compared to $C(0)$,

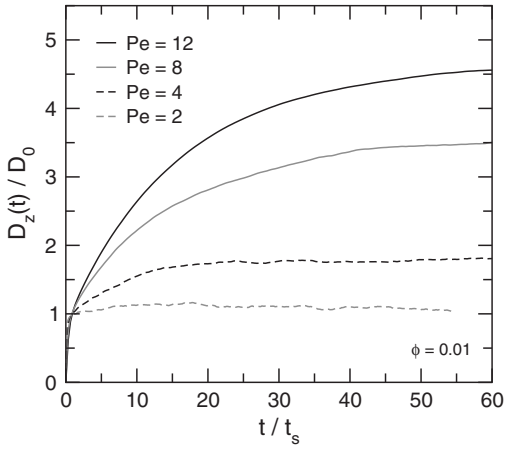

FIG. 9. Time-dependent self-diffusion coefficient parallel to gravity for different Pe numbers. D_0 is the equilibrium self-diffusion coefficient.

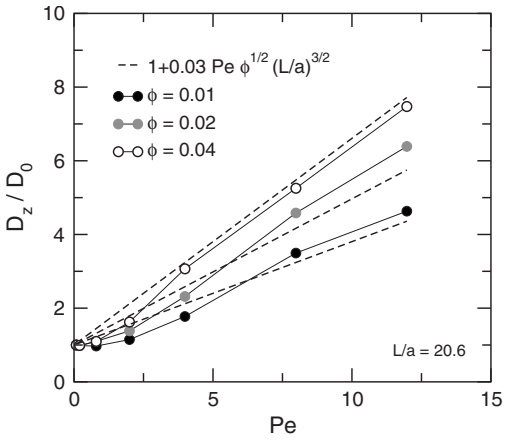

FIG. 10. Self-diffusion coefficient parallel to gravity versus Peclet number for different concentrations ϕ. D_0 is the equilibrium self-diffusion coefficient. Dashed lines are predictions from Eq. (19).

they nevertheless have a significant contribution to the diffusivity because the time-scale τ_H is much longer than τ_ν.

To understand the total diffusivity, we make the following addition approximation:

$$D_z = D_0 + D_H, \tag{17}$$

where D_0 is equilibrium diffusion coefficient and D_H the dispersion due to nonequilibrium hydrodynamic fluctuations. The former can be approximated as a sum of Stokes and Enskog diffusion coefficients, see [26]. The nonequilibrium hydrodynamic dispersion can be estimated using the previous scaling arguments,

$$D_H \approx \Delta V_H^2 \tau_H \propto V_S a \phi^{1/2} \left(\frac{L}{a}\right)^{3/2}. \tag{18}$$

Taking the prefactors found in the previous section, and rewriting $V_S a$ as Pe D_0, we therefore predict

$$D_z = D_0 \left[1 + 0.03 \text{ Pe } \phi^{1/2} \left(\frac{L}{a}\right)^{3/2}\right] \tag{19}$$

for small enough, i.e., unscreened, systems. For small Pe(<1) the self-diffusion coefficient is largely independent of Pe and equal to D_0, whereas for very large Pe($\gg 1$) it becomes proportional to Pe. This is confirmed in Fig. 10 where the dashed lines show the Pe and ϕ dependence of Eq. (19).

The diffusion in the plane perpendicular to gravity is also enhanced by the hydrodynamic fluctuations, similar to Eq. (19), but with a smaller prefactor of 0.004 instead of 0.03 (not shown). The ratio of hydrodynamic diffusivities, $D_H/D_{H,\text{perp}} \approx 7$ is similar to what is found in the experiments of Nicolai *et al.* [8] for non-Brownian spheres.

Although our simulations are in the unscreened regime, it is interesting to also consider the hydrodynamic contribution to the diffusion coefficient in the screened regime. If we apply the experimental fits of Segrè *et al.* [9] for ΔV_H and the correlation length ξ, then the simple scaling arguments above suggest that

$$D_H \propto \text{Pe } D_0, \tag{20}$$

which is *independent* of ϕ. The exact prefactor is hard to determine in the screened regime. Nevertheless, an estimate can be made if we assume that τ_H has the same prefactor in the experiments as we find in our simulations. For example, if we replace $L/2$, which measures the location of the minimum of the perpendicular correlation functions, with ξ_{perp}, its value for the screened regime [9], then we find $D_{H,\text{perp}}/D_0 \approx 1.1$ Pe. For $D_{H,\text{parallel}}/D_0$ we expect a prefactor several times larger. In the screened regime the hydrodynamic contributions to the diffusion should dominate for Pe$\gtrsim 1$. In practice, however, we expect that for many colloidal dispersions effects such as polydispersity [18] may temper the size of the swirls, and thus reduce the hydrodynamic contribution to diffusion. Similarly, for charged colloidal suspensions, the effects of salt, co- and counterions may also significantly temper the size of the hydrodynamic swirls [42–44].

VII. FINITE SEDIMENTATION IN A HORIZONTAL PLANAR SLIT

Up to this point we have focused on steady-state sedimentation by applying periodic boundary conditions and giving the system enough time to overcome transient flow effects.

One may wonder what happens if the particles are confined and are not given enough time to reach steady state. Very recently, Royall *et al.* [39] studied nonequilibrium sedimentation of colloids in a horizontal planar slit, at a Peclet number of order 1, using laser scanning confocal microscopy. Among other things, they measured the time evolution of the one-dimensional colloid density profile $\rho(z,t)$, where the z axis is normal to the horizontal plane. Two cases were considered. In the first case an initially homogenized sample was allowed to sediment to the bottom of the capillary. Good agreement was found with a dynamical density functional theory (DDFT) calculation that included a density-dependent mobility function. In the second case they considered an equilibrated sample turned upside down so that the previous sediment suddenly finds itself at the top of the capillary. In

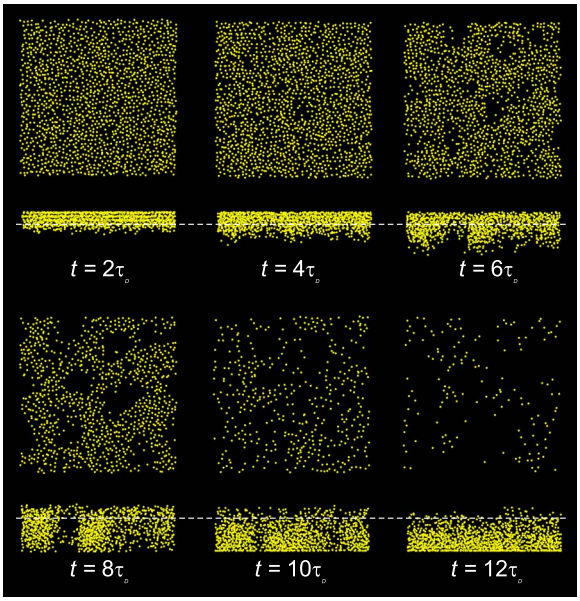

FIG. 11. (Color online) An equilibrated sediment in a planar slit is turned upside down and allowed to sediment at Pe=4. Shown here are the horizontal *xy* plane and the corresponding vertical *xz* plane at six different times after field reversal. The dashed line indicates the height *z* where the snapshots of the *xy* plane are taken. A strong fingerlike inhomogeneity develops quickly, accompanied by mazelike lateral pattern formation.

this case sedimentation proceeds in an entirely different fashion. A strong fingerlike inhomogeneity was observed, accompanied by mazelike lateral pattern formation.

Inspired by these experiments, we set up a box of size $180\times180\times60a_0$ $(116\times116\times39a)$, with periodic boundaries in the x and y direction, and with walls at the top and bottom in the z direction. (This corresponds to a height of about $32a$, close to the experimental value of $36a$.) We add 6500 colloids ($\phi\approx0.06$) and apply an external field upwards such that Pe=4. After reaching the equilibrium distribution, at $t=0$ we suddenly reverse the field, again at Pe=4. We observe a mazelike lateral pattern, Fig. 11 (most clearly visible at $t=8\tau_D$), which shows striking similarities to the experimental observations [39]. The characteristic length of the mazelike lateral pattern is approximately equal to the height of the slit. It has been suggested [39] that there may be a relation between this phenomenon and the swirls observed in steady-state sedimentation, but also that the swirls are reminiscent of a Rayleigh-Taylor-type instability in two layered liquids, with the steep initial density gradient resembling a (very diffuse) liquid-liquid interface. With the current data, we cannot conclusively determine the origin of this instability. Nevertheless it is gratifying that our simulations produce such similar, and nontrivial, behavior as the experiments under similar conditions. This can be viewed as an additional validation of our simulation model.

In Fig. 12 we analyze the time evolution of the one-dimensional density profile $\rho(z,t)$. The crystal-like layers at the top plate for $t<0$ disappear and then reappear again at the bottom of the plate. It would be interesting to compare these results to calculations using DDFT. Since the latter

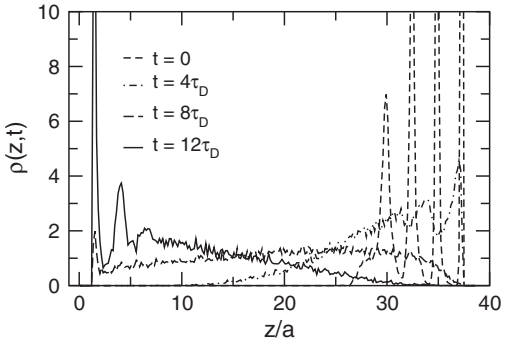

FIG. 12. Time evolution (right to left) of the one-dimensional density profile for sedimentation in a horizontal slit. ρ is normalized such that it equals 1 for a homogeneously filled slit. The final state (on the left) closely resembles the initial state (on the right), but is not shown for clarity.

technique does not explicitly contain any long-ranged hydrodynamics, one would expect it to have difficulty in reproducing the swirls observed in the simulations and experiments. Nevertheless, because both the initial and final states are constrained by equilibrium statistical mechanics (for which DFT is very accurate), the one-body density $\rho(z,t)$ may not be a very sensitive measure of the more complex dynamics that arise from hydrodynamics.

VIII. DISCUSSION

As seen in Fig. 6, the short time velocity fluctuations are dominated by thermal fluctuations at all Peclet numbers studied. The relative strength of the $t=0$ thermal and hydrodynamic velocity fluctuations follows from simple scaling relations. Using

$$\mathrm{Re\,Pe}=\frac{(V_S a)^2}{D_0\nu}, \tag{21}$$

which follows from the definitions of Pe and Re, together with Eqs. (6) and (13), the following relationship between hydrodynamic and thermal fluctuations emerges:

$$\frac{\Delta V_H^2}{\Delta V_T^2}\approx\alpha\,\mathrm{Re\,Pe}\,\phi\frac{L}{a}\frac{\rho_c}{\rho}\quad\text{(unscreened)}, \tag{22}$$

where the simplifying assumption that $M_c\approx\frac{4}{3}\pi\rho_c a^3$, with a the hydrodynamic rather than the physical radius, was also made. The numerical prefactor α is small and can be extracted from Fig. 8 to be $\alpha\approx0.05$ for fluctuations parallel to the flow, and $\alpha\approx0.015$ for fluctuations perpendicular to the flow.

The above scaling holds for the unscreened regime; in the screened regime the ratio of V_H to V_T will be smaller. Consider, for example, the experimental results of Segrè *et al.*[9]. If we take their fits to the scaling of the parallel fluctuations in the screened regime, together with the estimates $\mathrm{Re}=5\times10^{-5}$ and $\mathrm{Pe}\approx2000$, the scaling becomes

$$\frac{\Delta V_H^2}{\Delta V_T^2} \approx \phi^{2/3}\,\mathrm{Re\,Pe} \quad \text{(screened)} \tag{23}$$

for flows in the parallel direction. This suggests that this ratio is small in the experiments, from 2×10^{-4} for $\phi=10^{-4}$ to 0.02 for $\phi=0.1$. So despite the fact that the Pe number in these experiments appears to be high, there is no need for an effective gravitational "temperature" [10] to thermalize: at short correlation times the usual thermal fluctuations are still dominant. However, because the product Re Pe scales with quite a high power of a, as fast as a^7, the ratio $\Delta V_H^2/\Delta V_T^2$ will increase rapidly for larger particles and gravitational temperature will become essential for thermalization.

When comparing parallel and perpendicular components it is important to mention that in numerical works where thermal fluctuations are neglected very strong anisotropies in velocity fluctuations, hydrodynamic relaxation times, and diffusivities are often found. For example Ladd [40] finds $D_H/D_{H,\mathrm{perp}}\approx 25$ in his lattice Boltzmann simulations. This was attributed to periodic boundary conditions. However, we also use periodic boundary conditions and find results much closer to experimental results (a diffusivity ratio of $\sim$7). We therefore conclude that thermal fluctuations reduce the anisotropy. This could be tested in Lattice Boltzmann simulations by adding fluctuating stress [41,45].

IX. CONCLUSION

In conclusion, we have studied the interplay of hydrodynamic and thermal fluctuations using a simulation technique. The two types of fluctuations appear to act independently, at least in the unscreened regime. We find that hydrodynamic interactions are important for the average sedimentation velocity for Peclet numbers as low as 0.08, whereas thermal fluctuations may remain important up to very large Peclet numbers. Neither may be ignored for a significant range of Peclet numbers. We also calculate the hydrodynamic contributions to the diffusion coefficient, and find that with increasing Pe number they rapidly become much larger than the equilibrium diffusion coefficient. As an additional test of the method we studied finite sedimentation in a horizontal slit, and found characteristic lateral patterns in agreement with recent experiments.

ACKNOWLEDGMENTS

J.T.P. thanks the Netherlands Organisation for Scientific Research (NWO), and A.A.L. thanks the Royal Society (London) for financial support. We thank J. Hinch, R. Bruinsma, S. Ramaswamy, I. Pagonabarraga, W. Briels, and C. P. Royall for very helpful conversations.

[1] J. K. G. Dhont, *An Introduction to the Dynamics of Colloids* (Elsevier, Amsterdam, 1996).
[2] S. Ramaswamy, Adv. Phys. **50**, 297 (2001).
[3] W. B. Russell, D. A. Saville, and W. R. Showalter, *Colloidal Dispersions* (Cambridge University Press, Cambridge, England, 1989).
[4] G. G. Stokes, Trans. Cambridge Philos. Soc. **9**, 8 (1851); reprinted in *Mathematical and Physical Papers*, 2nd ed. (Johnson Reprint Corp., New York, 1966), Vol. 3.
[5] G. K. Batchelor, J. Fluid Mech. **56**, 245 (1972).
[6] H. Hayakawa and K. Ichiki, Phys. Rev. E **51**, R3815 (1995).
[7] R. E. Caflisch and J. H. C. Luke, Phys. Fluids **28**, 759 (1985).
[8] H. Nicolai, R. Herzhaft, E. J. Hinch, L. Oger, and E. Guazzelli, Phys. Fluids **7**, 12 (1995).
[9] P. N. Segrè, E. Herbolzheimer, and P. M. Chaikin, Phys. Rev. Lett. **79**, 2574 (1997).
[10] P. N. Segrè, F. Liu, P. Umbanhowar, and D. A. Weitz, Nature (London) **409**, 594 (2001).
[11] G. Bernard-Michel, A. Monavon, D. Lhuillier, D. Abdo, and H. Simon, Phys. Fluids **14**, 2339 (2002).
[12] S.-Y. Tee, P. J. Mucha, L. Cipelletti, S. Manley, M. P. Brenner, P. N. Segrè, and D. A. Weitz, Phys. Rev. Lett. **89**, 054501 (2002).
[13] M. P. Brenner, Phys. Fluids **11**, 754 (1999).
[14] D. L. Koch and E. S. G. Shaqfeh, J. Fluid Mech. **224**, 275 (1991).
[15] A. Levine, S. Ramaswamy, E. Frey, and R. Bruinsma, Phys. Rev. Lett. **81**, 5944 (1998).
[16] E. J. Hinch, in *Disorder and Mixing*, edited by E. Guyon, Y. Pomeau, and J. P. Nadal (Kluwer Academic Publishers, Dordrecht, Netherlands, 1988), p. 153.
[17] A. J. C. Ladd, Phys. Rev. Lett. **88**, 048301 (2002).
[18] N.-Q. Nguyen and A. J. C. Ladd, J. Fluid Mech. **525**, 73 (2005).
[19] P. N. Segrè, Phys. Rev. Lett. **89**, 254503 (2002).
[20] P. J. Mucha and M. P. Brenner, Phys. Fluids **15**, 1305 (2003).
[21] P. J. Mucha, S.-Y. Tee, D. A. Weitz, B. I. Shraiman, and M. P. Brenner, J. Fluid Mech. **501**, 71 (2004).
[22] P. N. Segrè and J. P. McClymer, J. Phys.: Condens. Matter **16**, S4219 (2004).
[23] L. Bergougnoux, S. Ghicini, E. Guazzelli, and J. Hinch, Phys. Fluids **15**, 1875 (2003).
[24] A. Malevanets and R. Kapral, J. Chem. Phys. **110**, 8605 (1999).
[25] T. Ihle and D. M. Kroll, Phys. Rev. E **67**, 066705 (2003); **67**, 066706 (2003).
[26] J. T. Padding and A. A. Louis, Phys. Rev. E **74**, 031402 (2006).
[27] A. Malevanets and R. Kapral, J. Chem. Phys. **112**, 7260 (2000).
[28] J. T. Padding and A. A. Louis, Phys. Rev. Lett. **93**, 220601 (2004).
[29] M. Hecht, J. Harting, T. Ihle, and H. J. Herrmann, Phys. Rev. E **72**, 011408 (2005).
[30] N. Kikuchi, C. M. Pooley, J. F. Ryder, and J. M. Yeomans, J. Chem. Phys. **119**, 6388 (2003).
[31] M. P. Allen and D. J. Tildesley, *Computer simulation of liquids* (Clarendon Press, Oxford, 1987).
[32] J. T. Padding, A. Wysocki, H. Löwen, and A. A. Louis, J. Phys.: Condens. Matter **17**, S3393 (2005).

[33] N.-Q. Nguyen and A. J. C. Ladd, Phys. Rev. E **66**, 046708 (2002).
[34] A. J. C. Ladd, Phys. Rev. Lett. **76**, 1392 (1996).
[35] G. Subramanian and H. T. Davis, Phys. Rev. A **11**, 1430 (1975).
[36] J. T. Hynes, Annu. Rev. Phys. Chem. **28**, 301 (1977).
[37] M. H. Ernst, E. H. Hauge, and J. M. J. van Leeuwen, Phys. Rev. Lett. **25**, 1254 (1970).
[38] F. R. Cunha, G. C. Abade, A. J. Sousa, and E. J. Hinch, J. Fluids Eng. **124**, 957 (2002).
[39] C. P. Royall, J. Dzubiella, M. Schmidt, and A. van Blaaderen, Phys. Rev. Lett. **98**, 188304 (2007).
[40] A. J. C. Ladd, Phys. Fluids **9**, 491 (1997).
[41] M. E. Cates, K. Stratford, R. Adhikari, P. Stansell, J.-C. Desplat, I. Pagonabarraga, and A. J. Wagner, J. Phys.: Condens. Matter **16**, S3903 (2004).
[42] H. Kodama, K. Takeshita, T. Araki, and H. Tanaka, J. Phys.: Condens. Matter **16**, L115 (2004).
[43] K. Kim, Y. Nakayama, and R. Yamamoto, Phys. Rev. Lett. **96**, 208302 (2006).
[44] F. Capuani, I. Pagonabarraga, and D. Frenkel, J. Chem. Phys. **124**, 124903 (2006).
[45] B. Dünweg, U. D. Schiller, and A. J. C. Ladd, Phys. Rev. E **76**, 036704 (2007).